Available online at www.sciencedirect.com
SCIENCE DIRECT®
Geochimica et Cosmochimica Acta 70 (2006) 1995–2005
Geochimica
www.elsevier.com/locate/gca

Geochemical chaos: Periodic and nonperiodic growth of mixed-layer phyllosilicates

Yifeng Wang [a,*], Huifang Xu [b]

[a] Sandia National Laboratories, P.O. Box 5800, Albuquerque, NM 87185-0776, USA
[b] Department of Geology and Geophysics, University of Wisconsin, Madison, Wisconsin 53706, USA

Received 9 May 2005; accepted in revised form 9 January 2006

Abstract

Interstratification—periodic or nonperiodic stacking of two different silicate layers along a c^*-axis—is common in phyllosilicates. Published evidence indicates that some interstratified minerals precipitate directly from aqueous solutions. In this paper, we have demonstrated, based on chaos theory, that both periodic and nonperiodic interstratification can autonomously arise from simple kinetics of mineral growth from a solution. Growth of a mixed-layer mineral is assumed to proceed layer by layer, and each layer starts with the formation of a base (Si, Al)–O tetrahedral sheet, whose structural configuration in *a*–*b* dimensions determines the type of new layer that forms. The sequence of layer stacking can be described by a one-dimensional map (i.e., a difference equation), which accounts for two competing factors: (1) the affinity of each end-member structural component for attaching to the surface of the preceding layer, and (2) the strain energy created by stacking next to each other two silicate layers with different structural configurations. Chaotic (or nonperiodic) interstratification emerges when the contacting solution becomes slightly supersaturated with respect to both structural components. The transition from one interstratification pattern to another reflects a change in chemical environment during mineral crystallization. Our model can successfully predict the occurrence of mixed-layer phyllosilicates and the associated layer stacking sequences observed in both hydrothermal alteration and sediment diagenesis. The model suggests that the diagenetic transition of smectite → nonperiodic illite/smectite → ordered illite/smectite → illite may reflect relative changes in the saturation degree of pore water with respect to two end-member phases as a result of increasing burial temperatures.

1. Introduction

Interstratification in phyllosilicates involves stacking of two different silicate layers (or silicate-plus-hydroxide layers) either periodically or nonperiodically along a c^*-axis. Periodic layer stacking has been reported for various series of phyllosilicates: illite–smectite (e.g., Nadeau et al., 1984; Ahn and Peacor, 1986; Eberl et al., 1990; Veblen et al., 1990), chlorite-talc (Schreyer et al., 1982), chlorite–pyrophyllite (Kong et al., 1990), smectite–illite (Veblen et al., 1990), chlorite–smectite (Hiller, 1993), chlorite–serpentine (Bailey et al., 1995; Xu and Veblen, 1996), smectite–pyrophyllite (Dong et al., 2002), and chlorite–biotite (Eroshchev-Shak, 1970; Xu et al., 1996). In contrast, nonperiodically interstratified silicate layers, not considered as independent mineral species, have received less attention, although their occurrences are probably more abundant than the periodic ones (e.g., Xu et al., 1996). Nonperiodic layer stacking is common in illite–smectite (e.g., Niu et al., 2000; Olives et al., 2000), chlorite–biotite (e.g., Veblen and Ferry, 1983; Eggleton and Banfield, 1985; Xu et al., 1996), corrensite–chlorite (e.g., Bautier et al., 1995), kaolinite–smectite (e.g., Dekov et al., 2005), and chlorite–wonesite series (Veblen, 1983). Systematic structural transition from nonperiodic to periodic layer stacking has been found in the conversion of smectite to illite in sediment diagenesis (e.g., Niu et al., 2000; Inoue et al., 2004). Transmission electron microscopy (TEM) studies have further revealed that the structural domains

* Corresponding author. Fax: +1 505 284 4002.
E-mail address: ywang@sandia.gov (Y. Wang).

0016-7037/$ - see front matter © 2006 Elsevier Inc. All rights reserved.
doi:10.1016/j.gca.2006.01.002

with different interstratification patterns coexist even in a single layer sequence (Schreyer et al., 1982; Ahn and Peacor, 1986; Kong et al., 1990; Veblen et al., 1990; Xu et al., 1996).

Several hypotheses have been proposed for the formation of interstratified phyllosilicates. Zen (1967) developed the Axial Next-Nearest-Neighbor Ising (ANNNI) model based on the assumption of a periodically interstratified silicate as a thermodynamically stable phase. A similar model was proposed by Blanc et al. (1997) based on short-range interactions. Interstratified phases have also been considered as intermediate structures of solid-state transformation from one layered silicate to another (Hower et al., 1976; Maresch et al., 1985). Nadeau et al. (1984) proposed that interstratification might result from precipitation of "fundamental particles." Periodic arrangements arise from homogeneous particle populations and nonperiodic arrangements from heterogeneous populations. For example, for the illite–smectite series, R1 ordering (ISISIS) would be produced if 2-nm particles dominate a particle suspension; similarly, R2 ordering (IISIIS) would be generated if 3-nm particles dominate (Środoń, 1999; Środoń et al., 2000). Kong et al. (1990) attributed periodic interstratification to an externally forced periodic oscillation in solution chemistry. Xu et al. (1996) extended this concept to explain the transition from periodic to nonperiodic interstratification in the chlorite–biotite series by arguing that, with an increase in the amplitude of oscillations, their nonlinear crystallization model could shift from a periodic to a nonperiodic regime. Such models, however, have an inherent difficulty: lack of any plausible external force that can generate oscillations on an appropriate scale for interstratification.

The origins of mixed-layer minerals still remain controversial (see a comprehensive review by Środoń, 1999). Much of the controversy stems from the degree of the involvement of aqueous solutions in mineral reactions, possibly ranging from pure solid-state transformation to direct precipitation from aqueous solutions (Altaner and Ylagan, 1997). Evidence suggests that, at least in some cases, aqueous solutions play an important role in the formation of interstratified minerals. For example, Alt and Jiang (1991) have demonstrated that illite–smectite mixed layers present as a pore filling in recent massive sulfide deposits from a seamount near the East Pacific Rise must have precipitated directly from hydrothermal fluids. Similarly, Xu et al. (1996) reported the occurrence of chlorite–biotite mixed layers as a vein filling in a hydrothermally alterated norite. It is even suggested that the conversion of smectite to illite in sediment diagenesis may have also undergone a dissolution–precipitation process (e.g., Lynch et al., 1997; Niu et al., 2000; Inoue et al., 2004; Dong, 2005).

While recognizing potential multiple origins of mixed-layer phyllosilicates, in this paper, we focus exclusively on the mixed layers that directly precipitate from aqueous solutions. We show that both periodic and nonperiodic interstratification in these minerals is a chaotic phenomenon autonomously arising from simple kinetics of mineral growth without any outside influence. We demonstrate that, as a controlling parameter changes, the system can shift from periodic to nonperiodic layering through period-doubling bifurcations. Thus, the transition from one layer-stacking pattern to another reflects a change in chemical environment during mineral growth.

2. TEM observations

We use the chlorite $[Al_{4.33}(Si_3Al)O_{10}(OH)_8]$–pyrophyllite $[Al_2Si_4O_{10}(OH)_2]$ series as an example to show typical layer-stacking patterns in phyllosilicates. The samples investigated for this study were collected from a pyrophyllite mineral deposit in Qingtian, Zhejiang Province, China. The mineral deposit is considered to be formed by hydrothermal alteration of upper Jurassic rhyolitic volcanic rocks. The samples containing interstratified chlorite–pyrophyllite were taken from the western part of the deposit, which is dominated by pyrophyllite, sericite, and chlorite. Small amounts of corundum and diaspore are also present. Both the field and optical microscopic observations indicate that the interstratified chlorite–pyrophyllite must have crystallized directly from Al-rich hydrothermal solutions with a sequence of corundum → diaspore → chlorite/pyrophyllite. The specimens for TEM investigation were selected from petrographic thin sections and thinned to electron transparency with a Gatan ion mill. All the specimens were examined using a JEOL 2010 high-resolution TEM associated with an ISIS EDS system from Oxford Instruments.

Electron diffraction and high-resolution TEM (HRTEM) analyses indicate the presence of both periodically and nonperiodically interstratified chlorite–pyrophyllite in the samples (Fig. 1). The nonperiodic-structure domains coexist with the periodic-structure domains as well as the domains dominated by either chlorite or pyrophyllite layers. The transition from one interstratification pattern to another is illustrated in Fig. 1 (lower panels). The selected-area electron diffraction (SAED) pattern (with *00l* diffraction only) of a domain dominated by nonperiodic layer stacking is shown in Fig. 2. Nonperiodic interstratification contributes to the streaking of the *00l* along the c^*-axis in the SAED patterns. The feature of *00l* diffraction rows is different from the feature of either periodic or purely random oscillations in a spectrum space (Fig. 2), indicating the possible existence of chaotic layer sequences (Baker and Gollub, 1990).[1] In this paper, we use terms "nonperiodic" and "chaotic" interchangeably. The SAED pattern indicates a period of 23.4 Å along the c^*-axis. The 23.4 Å periodicity equals the sum of d_{001} values of chlorite (14.2 Å) and pyrophyllite (9.2 Å). In the sample examined, the nonperiodic layers appear more abundant than their

[1] Note that chaos, as opposed to "randomness," has its "order" or "determinism" in the underlying complex dynamics (Sprott, 2003).

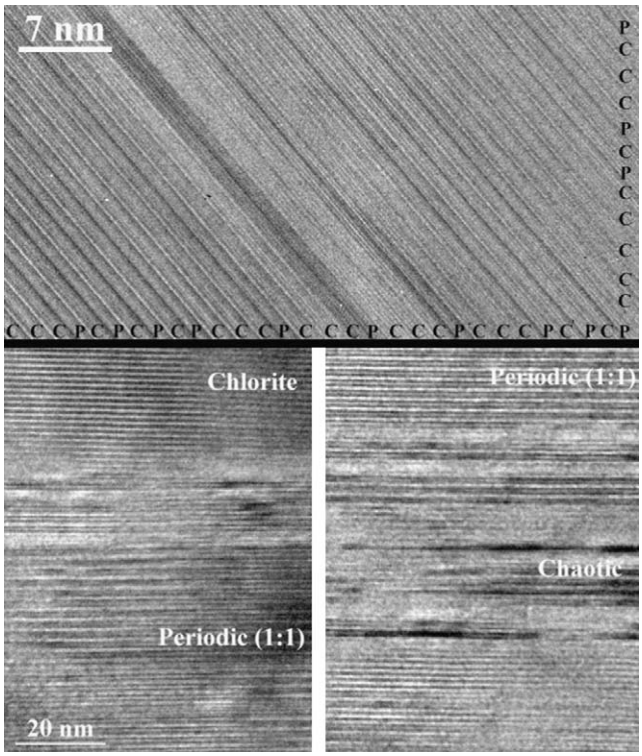

Fig. 1. HRTEM images of interstratified chlorite–pyrophyllite series. Chlorite (C) and pyrophyllite (P) layers are nonperiodically stacked along c^*-axis (upper panel). Nonperiodic (or chaotic) structure domains appear intergrown with the periodic structure domains as well as the domains dominated by end-member phases (lower panels).

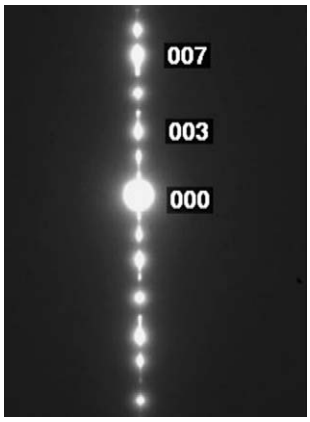

Fig. 2. Selected-area electron diffraction pattern (with *00l* diffraction only) of the mixed-layer pyrophyllite/chlorite showing diffraction maximum and streaking diffraction caused by intergrowth of periodic and non-periodic domains. The positions of 003 and 007 reflections of the 1:1 periodic domain are also labeled.

periodic counterparts. A similar observation has been made for chlorite–biotite systems (Xu et al., 1996).

An electron microprobe analysis shows that interstratified phyllosilicates are heterogeneous in chemical composition (Fig. 3). The composition varies from area to area even within a "single crystal." The molar fraction of pyrophyllite in the interstratified crystals ranges from 0.23 to 0.46. This

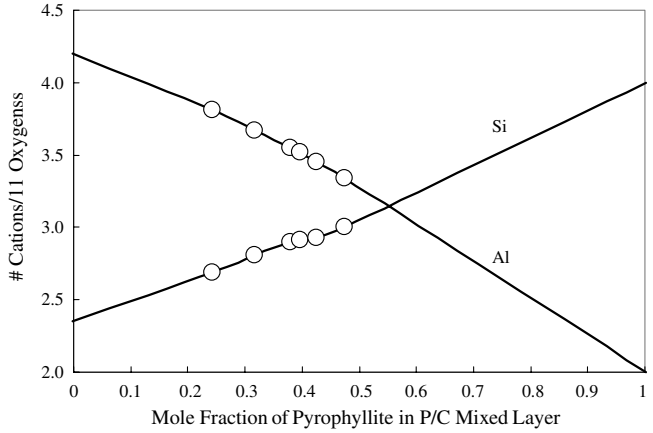

Fig. 3. Compositional variations within a single interstratified crystal as revealed by an electron microprobe analysis. The data indicate chemical heterogeneity in interstratified chlorite (C)–pyrophyllite (P) minerals.

compositional heterogeneity is due to the presence of either different ratios of end-member layers in the probed areas or variable layer compositions as discussed in Section 4.5 below. Since a single electron microprobe analysis encompasses a large number of individual silicate layers, these analyses alone do not allow us to discern the dominant factor for the observed heterogeneity. The interstratified chlorite–pyrophyllite crystals display interference colors of second-order purple in relatively homogeneous (probably periodic) areas and first-order gray and white in heterogeneous (probably nonperiodically interstratified) areas.

As shown above, TEM imaging allows a direct observation of local layer sequences on a scale of individual silicate layers. While, in many cases, the information on mineral interstratification is obtained with powder X-ray diffraction (XRD), which only provides a statistical measurement of layer ordering in bulk samples. Thus, a partially ordered bulk sample may contain both periodic and nonperiodic local sequences. As the proportion of nonperiodic local sequences increases, the bulk sample becomes more deviated from the property of regular ordering. This correlation provides a basis for applying our chaos model to diagenetic transition of smectite to illite, for which most layer stacking information has been obtained with powder XRD in bulk samples (e.g., Środoń, 1999; Inoue et al., 2004). Our model proposed below is based on local layer sequences.

3. Autonomous chaos model

3.1. Model assumption

Chaos theory deals with the behavior of certain nonlinear dynamic systems that, under certain conditions, exhibit the phenomenon known as chaos. Behaviors of a chaotic system are aperiodic. Such behaviors arise even though the system is 'deterministic' in the sense that it is well defined and contains no random parameters (e.g., Strogatz, 1994). Chaos theory thus points out the possibility that the complexity of a dynamic system can emerge from its

internal nonlinear deterministic dynamics. A chaotic behavior is different from purely random variations (i.e., white noise), and chaos has its own underlying structures (e.g., Sprott, 2003). Chaos theory has been exploited to understand the irregular behaviors and the unpredictability of various geophysical processes such as faulting, seismic events, rainfall, river flow, and sediment transport (e.g., Huang and Turcotte, 1990, 1992; Sivakumar, 2004). We here propose a deterministic chaos model for the formation of interstratified phyllosilicates. To our knowledge, this is the first time that such concept has been applied to mineral growth.

The layered structures of phyllosilicates are expected to impose a unique constraint on the growth of these minerals. Let's use the pyrophyllite–Al-chlorite series as an example. Each pyrophyllite layer $[Al_2Si_4O_{10}(OH)_2]$ consists of a sheet of octahedrally coordinated Al ions sandwiched between two sheets of linked Si–O tetrahedra. Each Al-chlorite layer contains a similar silicate layer $[Al_2(Si_3Al)O_{10}(OH)_2]$ with 1/4 of Si in the tetrahedral sheet replaced with Al and with an additional brucite-like sheet $[Al_{2.33}(OH)_6]$ added on the top of each layer. It is reasonable to expect that crystallization of a mixed-layer mineral from an aqueous solution proceeds by successively adding silicate layers to a growing surface perpendicular to the c^*-axis. Growth of a new silicate layer starts with the formation of a sheet of (Si, Al)–O tetrahedra by attaching tetrahedrally coordinated Si or Al ions onto the growing surface. This tetrahedral sheet, common to both end-member layers, constitutes the bottom sheet of a new layer that forms, and we hereafter refer this sheet as the base T-sheet. The (Si, Al)–O tetrahedra in this base T-sheet are linked to form pseudo-hexagonal (or di-trigonal) rings, which generally exhibit distinct geometric configurations in the two end-member phases of a mixed-layer mineral. For example, the rings in pyrophyllite are more distorted than those in chlorite (Evans and Guggenheim, 1988; Bailey, 1988). We assume that the structural configuration of the base T-sheet directly determines the type of silicate layer to form for a new layer. The structural configuration is characterized by the relative proportions of two sets of pseudo-hexagonal rings with distinct geometric distortion or equivalently the degree of distortion of the rings relative to those in the two end-member phases (Xu et al., 1996). For convenience, we hereafter refer each set of these hexagonal rings as a structural component, A or B, with emphasis on their difference in geometry. Since this geometric difference is generally small, structural components A and B can be easily accommodated without inducing any incoherent boundary between the two components within the base T-sheet. We thus expect that the molar fraction of each structural component in the base T-sheet can vary continuously over the range of 0–1 from one silicate layer to another. After attachment of the base T-sheet, the rest of the layer (e.g., an octahedral sheet followed by another tetrahedral sheet for a pyrophyllite layer) is immediately added on the top of the base T-sheet in order to minimize charge imbalance on the growing surface. The type of sheets to be added depends on the structural configuration of the base T-sheet. A new silicate layer of type A forms if the structural component A dominates the base T-sheet; and otherwise a new layer of type B precipitates.

The actual process of layered-mineral growth is perhaps more complex than that described above. It is possible, for instance, that other common sheets such as the overlaying octahedral sheet (O-sheet) may form simultaneously with the base T-sheet. The type of new layer that forms is then determined by the structural configuration in a–b dimensions of all these sheets, which can still be characterized by the geometry of (Si, Al)–O hexagonal rings in the base T-sheet.

Without delving into details of layered-mineral growth, which to a large part still remain unknown, we assume, based on phenomenological considerations, that the relative proportion of each structural component in the base T-sheet is controlled by two competing factors: the saturation degree of the solution with respect to each structural component and the strain energy created by stacking next to each other the two silicate layers with different structural configurations in a–b dimensions.

3.2. Mathematical model

The rate of a structural component attaching to the surface of a preceding silicate layer is driven by the tendency (i.e., chemical affinity) for the formation of the corresponding end-member mineral phase from the contacting solution. That is, the higher the supersaturation of the solution is with respect to an end-member phase, the higher attachment rate would be expected for the corresponding structural component. We assume that this attachment process follows a simple kinetic law (e.g., Lasaga, 1981):

$$R_A = k_A(\Omega_A - X_{i-1}), \tag{1A}$$

$$R_B = k_B(\Omega_B - Y_{i-1}), \tag{1B}$$

where R_A and R_B are the rates of components A and B attaching onto the growing surface upon the initiation of layer i, respectively; k_A and k_B are the rate constants of the attachment reactions; Ω_A and Ω_B are the saturation degrees of solution with respect to structural components, A and B, respectively; X_i and Y_i are the molar fractions of components A and B in the base T-sheet of layer i, with $X_i + Y_i = 1$. The terms in the parentheses represent the chemical affinity for the precipitation of each structural component. The molar fraction of structural component A in the base T-sheet of layer i is then expected to be proportional to the relative attachment rates of the two structural components

$$X_i \propto \frac{R_A}{R_A + R_B} = \frac{k_A(\Omega_A - X_{i-1})}{k_A(\Omega_A - X_{i-1}) + k_B(\Omega_B - Y_{i-1})}. \tag{2}$$

As more A and B structural units are added to the surface, the strain between two structural components both within the base T-sheet and between the base T-sheet and its underlying substrate becomes more pronounced. In principle, this energy can be calculated with lattice-energy models (e.g., Olives et al., 2000). However, to keep our model tractable, we use the following phenomenological expression to capture the essence that the strain energy tends to force the system to precipitate the like structural component

$$X_i \propto X_{i-1}. \tag{3}$$

A similar expression was used for modeling oscillatory zoning in plagioclase feldspar (Hasse et al., 1980).

Combining Eqs. (2) and (3), we finally obtain a kinetic model for the precipitation of a mixed-layer phyllosilicate

$$X_i = f(X_{i-1}) = \frac{\alpha X_{i-1}(\Omega_A - X_{i-1})}{(\Omega_A - X_{i-1}) + \gamma(\beta\Omega_A + X_{i-1} - 1)}, \tag{4}$$

where α is the proportionality constant; $\gamma = k_B/k_A$; and $\beta = \Omega_B/\Omega_A$. As shown in Section 4.1, α ranges from 3.5 to 4 for chaotic behaviors. If the mineral growth were only controlled by the saturation degree of solution, α should be one (Eq. (2)). Thus, to a large extent, α reflects the degree of dissimilarity between the two structural components involved in interstratification. Eq. (4) is a one-dimensional map. As γ, Ω_A and $\Omega_B \to 1$, the equation is reduced to a standard logistic equation, $X_i = \alpha X_{i-1}(1 - X_{i-1})$, which has been used to describe population dynamics and shown to exhibit rich chaotic behaviors (May, 1976).

To ensure $0 \leqslant X_i \leqslant 1$, it is required that

$$\Omega_A, \Omega_B \geqslant 1, \tag{5}$$

$$\frac{(\alpha\Omega_A - \gamma + 1)^2}{4\alpha} \leqslant \Omega_A + \gamma(\beta\Omega_A - 1). \tag{6}$$

These conditions delineate a physically meaningful parameter space, in which the dynamic behavior of the system can be studied. A linear stability analysis (e.g., Strogatz, 1994; Merino and Wang, 2000) of Eq. (4) shows that the system becomes unstable (a necessary condition for both periodic and nonperiodic layer stacking) if

$$\lambda = \left| \frac{\alpha(\Omega_A - 2\overline{X})[\Omega_A - \overline{X} + \gamma(\beta\Omega_A + \overline{X} - 1)] - \alpha(\Omega_A - \overline{X})\overline{X}(\gamma - 1)}{[\Omega_A - \overline{X} + \gamma(\beta\Omega_A + \overline{X} - 1)]^2} \right| > 1, \tag{7}$$

where $\overline{X}$ is a steady-state solution of Eq. (4) calculated by

$$\overline{X} = \frac{(\alpha - 1)\Omega_A - \gamma(\beta\Omega_A - 1)}{\alpha + \gamma - 1}, \tag{8}$$

and $\lambda = |f'(\overline{X})|$ and is a multiplier for the growth of a small perturbation around the steady state. The perturbation tends to grow (i.e., the system becomes unstable) if $\lambda > 1$. The unstable domain can be further differentiated by the Lapunov exponent (Strogatz, 1994; p. 367),

$$L = \lim_{n\to\infty} \left\{ \frac{1}{n} \sum_{i=0}^{n-1} \ln|f'(X_i)| \right\} > 0 \quad \text{for chaotic layer stacking} \tag{9}$$

in combination with model simulations. The resulting phase diagrams are shown in Fig. 4. The behavior domains

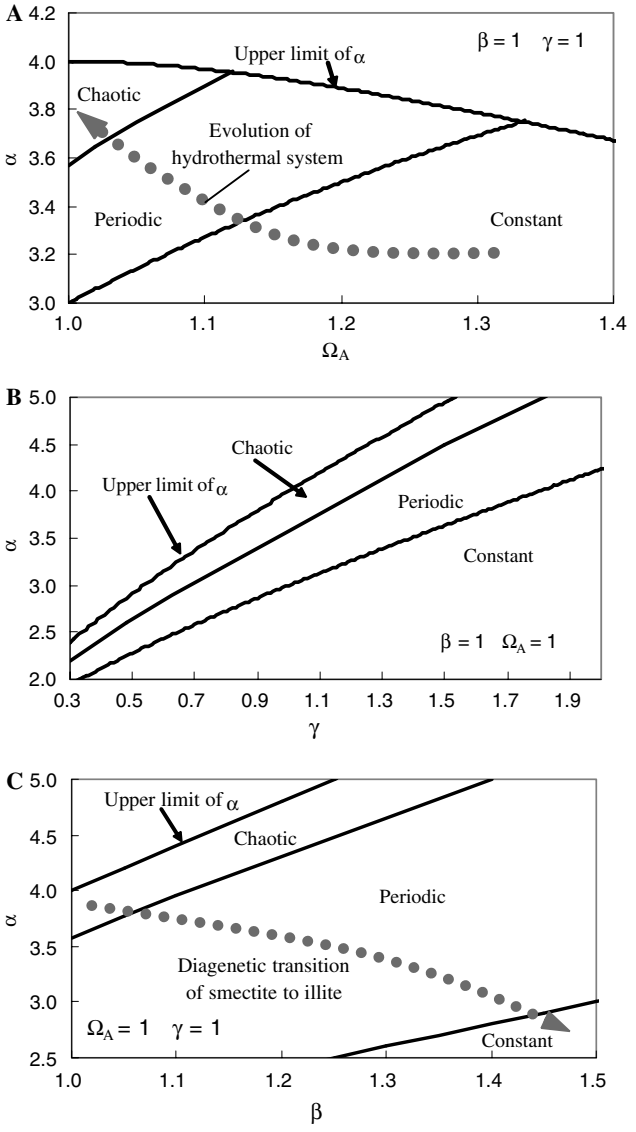

Fig. 4. Phase diagrams delineating the growth behaviors of a mixed-layer phyllosilicate in a parameter space. The behavior domains are determined as follows: constant ($\lambda < 1$ and $L < 0$), periodic ($\lambda > 1$ and $L < 0$), and chaotic ($\lambda > 1$ and $L > 0$). The "constant" domain refers to the formation of an end-member phase. Chaotic interstratification occurs when the saturation degree of the solution approaches one with respect to both structural components. The upper limit of α is constrained by Eq. (6). Note that α decreases with increasing temperature. Also note that the evolution of a hydrothermal system toward chemical equilibrium is generally associated with a temperature decrease, while in sediment diagenesis the change in relative saturation degree between two structural components is induced by an increase in burial temperature. The transitions of layer-stacking patterns in hydrothermal alteration (A) and sediment diagenesis (C) are indicated by broken arrow lines, which account for the changes in both saturation degree and temperature.

are determined as follows: constant ($\lambda < 1$ and $L < 0$), periodic ($\lambda > 1$ and $L < 0$), and chaotic ($\lambda > 1$ and $L > 0$). The "constant" domain refers to the formation of an end-member phase.

4. Results and discussion

4.1. Phase diagrams

As discussed above, α reflects the degree of dissimilarity between the two structural components involved in interstratification. As shown in Fig. 4, for chaotic layer stacking, α is required to be above a critical value, implying that a certain degree of dissimilarity between the structural components promotes nonperiodic interstratification. However, this dissimilarity cannot be too large; otherwise it would result in the formation of separated end-member phases only. An optimal α value for chaotic interstratification is expected to be such that the contribution of the strain energy is just high enough to interplay with the solution saturation degree. This prediction seems consistent with the observations that irregular interstratification is common in illite–smectite, chlorite–pyrophyllite, chlorite–biotite, chlorite–berthierine, and pyrophyllite–smectite series (e.g., Xu and Veblen, 1996; Xu et al., 1996; Środoń, 1999; Dong et al., 2002), in which the structural components (i.e., the structural configurations in *a–b* dimensions) of end-member layers are distinct but sufficiently similar. A quantitative evaluation of this similarity (or dissimilarity) requires calculating lattice energy changes due to the stacking of two different silicate layers and comparing the calculation results with the observed occurrence of different combinations of these layers in interstratified phyllosilicates. Such calculations are beyond our model capabilities.

It is reasonable to expect that the small difference between the two structural components is not sufficient to change the nature of the attachment of each component onto a growing surface. Therefore, the ratio of reaction constants, γ, in Eq. (4) should be close to 1. From Fig. 4B, the optimal α value for chaotic layer stacking then falls in the range of 3.5–4.0. Note that parameter α is also temperature dependent. At a higher temperature, the dissimilarity between the two structural components would become less important because the mineral structures generally become more tolerant to distortion and mismatches. Therefore, the α value is expected to decrease with temperature.

Parameters Ω_A and β deserve specific discussion, because, for a given mixed-layer phyllosilicate, the saturation degree of the solution is a main factor controlling the transition of interstratification patterns. Together with Eq. (5), Figs. 4A and C suggest that chaotic layer stacking takes place when the solution is either in equilibrium or slightly supersaturated with both structural components. This is because, as discussed above, the supersaturation of the solution, if it is too high, would overwhelm the effect of the structural strain energy. This prediction is consistent with the observation that nonperiodic-layering domains generally coexist with the domains of two end-member phyllosilicates (Fig. 1, lower left panel). Since many geochemical systems such as hydrothermal systems would eventually evolve toward equilibrium, the occurrence of chaotic layer stacking is expected to be common, as observed (e.g., Xu et al., 1996).

A transition from one layer-stacking pattern to another can result from changes in either the overall (Ω_1 and Ω_2) or the relative (β) saturation degree of the solution with respect to the two structural components (Figs. 4A and C). As shown below, these two transition pathways represent the evolution of interstratified phyllosilicates in a hydrothermal system and during sediment diagenesis, respectively. In an actual geochemical system, the evolution of solution chemistry is generally associated with temperature changes. For example, in a hydrothermal system, the temperature usually decreases as the system evolves toward chemical equilibrium. In sediment diagenesis, the increase in burial temperature directly controls the relative saturation degree of two structural components in pore waters (e.g., Inoue et al., 2004 and detail discussion below). The evolution pathways of mineral structure for hydrothermal alteration and sediment diagenesis shown in Figs. 4A and C are constructed by taking into account the effects of both saturation degree and temperature changes. Note that parameter α decreases with temperature, as discussed above.

4.2. Nonperiodic layer stacking through bifurcations

Fig. 5 shows a typical evolution pathway of a hydrothermal system with an initial solution highly saturated with both structural components. As the system evolves toward equilibrium, a successive transition of layer-stacking patterns is induced (Fig. 5A): no interstratification → periodic interstratification → nonperiodic interstratification. As shown in Fig. 5B, such transition arises from period-doubling bifurcations, through which the number of unstable steady states of the system are successively doubled as a controlling parameter, here the saturation degree of the solution, is smoothly varied. Fig. 5B is constructed from numerical simulations of Eq. (4). Our model has thus demonstrated that both periodic and nonperiodic interstratification in phyllosilicates can autonomously emerge from a simple deterministic mechanism of mineral growth without any outside influence. In this sense, periodic interstratification is a self-organizational phenomenon (Wang and Merino, 1992, 1993, 1995). Interestingly, our model indicates that a variety of periodically interstratified phyllosilicates, traditionally considered as independent mineral species, may form before the system becomes completely chaotic. Thus, from a point of view of bifurcation, periodically interstratified phyllosilicates are the intermediate phases of the transition from no interstratification to chaotic interstratification.

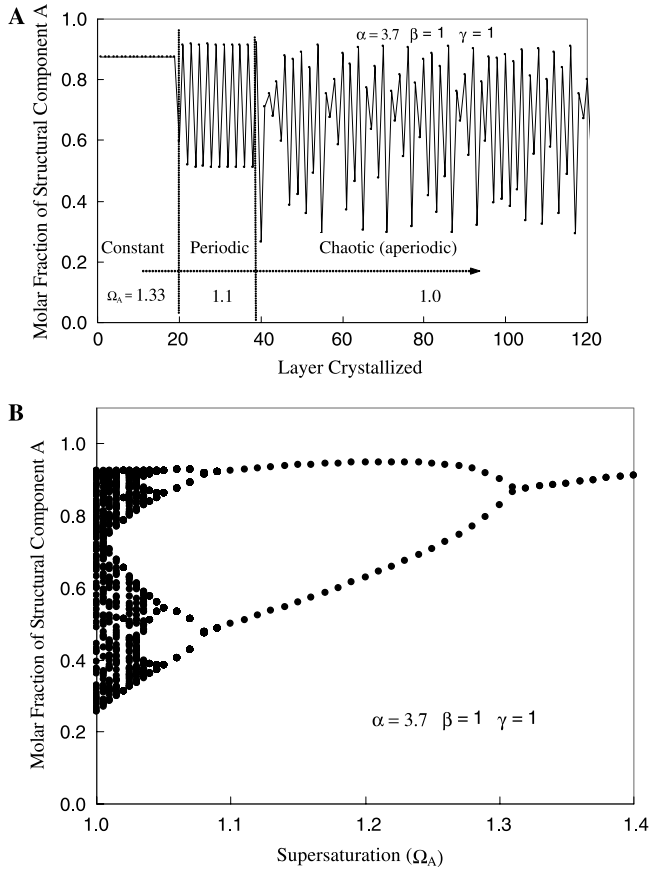

Fig. 5. Transition of layer-stacking patterns through bifurcations. (A) Successive transition of layer-stacking pattern as a hydrothermal system evolves from being highly saturated toward equilibrium: no interstratification → periodic interstratification → nonperiodic interstratification. (B) Chaotic layer stacking arising from period-doubling bifurcations.

The chaotic behavior of Eq. (4) can be further studied in a so-called time-delay embedding space (Sprott, 2003), which is generally used to reveal underlying structures of a chaotic sequence. X_i is plotted against X_{i-1} in Fig. 6. It can be seen in the figure that Eq. (4) displays a unique chaotic characteristic different from other known one-dimensional maps (Sprott, 2003, pp. 717–721). Apparently, it behaves differently from the standard logistic equation.

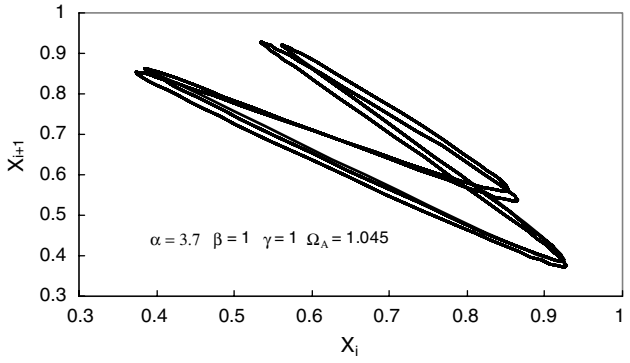

Fig. 6. Chaotic behavior of Eq. (4) revealed in a time-delay embedding space.

4.3. Formation of interstratified phyllosilicates in hydrothermal systems

The above discussion allows us to construct a possible evolution pathway for the chlorite–pyrophyllite system we have studied (Fig. 7). The presence of corundum (Al_2O_3) crystals in the sample indicates that the hydrothermal system was initially far from equilibrium with both chlorite and pyrophyllite. According to Figs. 4A and 5A, as chlorite, pyrophyllite, and other silicate minerals precipitated, the chemical system moved toward the eutectic point of chlorite and pyrophyllite, resulting in the formation of both periodically and nonperiodically interstratified phyllosilicates. This predicted sequence still needs to be confirmed by detail petrographic and TEM studies. Nevertheless, it seems consistent with the observations of other hydrothermal systems. Alt and Jiang (1991) observed that the evolution of smectite to illite in recent massive sulfide deposits from a seamount near the East Pacific Rise might not follow a general diagenetic sequence of smectite → random illite/smectite → ordered illite/smectite → illite (see discussion below). Their observations indicate direct precipitation of R1 illite/smectite mixed layers from hydrothermal solutions. Such "anomalous" pre-

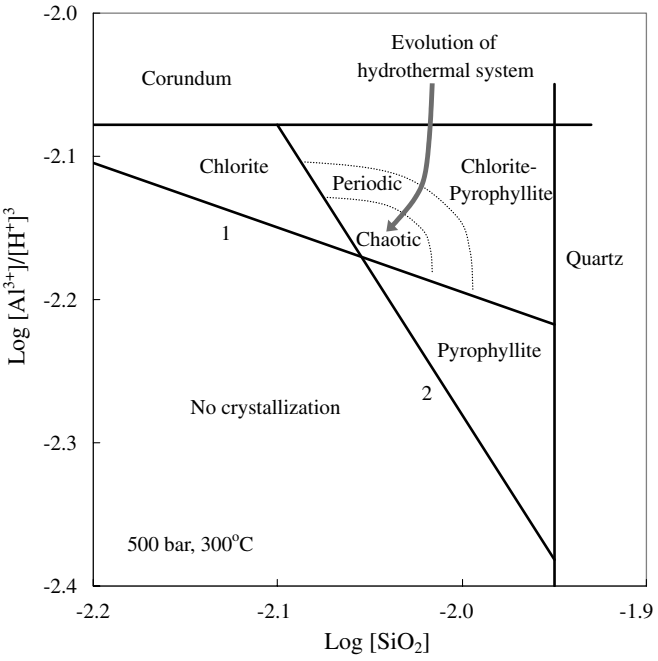

Fig. 7. Schematic representation of the evolution of chlorite–pyrophyllite system postulated from our TEM observations and model simulations. The arrow indicates the evolution of hydrothermal fluid composition. Chaotic interstratification tends to occur near the eutectic point of chlorite and pyrophyllite reactions: (1) $3SiO_{2(aq)} + 5.33Al^{3+} + 12H_2O = Al_{4.33}(Si_3Al)O_{10}(OH)_8 + 16H^+$ and (2) $4SiO_{2(aq)} + 2Al^{3+} + 4H_2O = Al_2Si_4O_{10}(OH)_2 + 6H^+$. Data for corundum, pyrophyllite, and quartz are from Berman (1988). The slope for chlorite is based on the stoichiometry of chlorite. The intercept for the chlorite line is chosen such that Al-chlorite can coexist with pyrophyllite. The temperature of 300 °C and the pressure of 500 bar are chosen to represent a typical hydrothermal environment.

cipitation is very likely, according to our model, as the hydrothermal system evolves from being highly supersaturated to an equilibrium state (Fig. 4A). In this case, ordered illite/smectite mixed layers can precipitate earlier than their random counterparts.

4.4. Smectite–illite conversion in sediment diagenesis

As shown in Fig. 4C, the transition of layer-stacking patterns can also result from the changes in the ratio of saturation degree between two structural components. Such transition can be best illustrated with the conversion of smectite to illite in sediment diagenesis. This conversion has been extensively studied during the last half century (e.g., Burst, 1959; Hower et al., 1976; Eberl et al., 1990; Alt and Jiang, 1991; Lynch et al., 1997; Niu et al., 2000; Inoue et al., 2004). Mineralogical and structural changes associated with this conversion have been well documented (e.g., Środoń and Eberl, 1984; Lynch et al., 1997; Niu et al., 2000; Inoue et al., 2004). As illustrated in Fig. 8, as the burial temperature increases, phyllosilicate minerals in sediments undergo the following systematic changes: smectite (zone I) → nonperiodic illite–smectite (zone II-A) → periodic illite–smectite (II-B) → illite (III).

Assume that the conversion of smectite to illite involves a dissolution-precipitation process (e.g., Eberl et al., 1990; Lynch et al., 1997; Niu et al., 2000; Inoue et al., 2004; Dong, 2005). Also, assume that the stabilities of smectite and illite change oppositely with temperature, with illite more stable at elevated temperatures (Inoue et al., 2004). Based on these assumptions, our model is able to predict the observed smectite–illite transition sequence. As illustrated in Fig. 8, in zone I, the dissolution of detrital felsic minerals causes the pore water to be slightly supersaturated with the smectite component, while the illite component remains undersaturated due to low temperatures. As a result, only smectite precipitates because the conditions in Eq. (5) are not satisfied. With a further increase in temperature, the pore water becomes equally saturated with both smectite and illite components in zone II-A, and the chemical system enters the chaotic domain in Fig. 4C. Nonperiodic interstratification results. As illite becomes more saturated, the ratio of saturation degree between smectite and illite, β, increases, which forces the chemical system to move away from the chaotic domain into the periodic region (Fig. 4C), resulting in the formation of ordered mixed-layer minerals. And finally, after all felsic minerals and smectite are completely dissolved, the pore water becomes undersaturated with smectite, and Eq. (5) no longer holds. Consequently, only illite forms in zone III. The relative abundance of each mineral structure in each zone apparently depends on a specific burial/thermal history of sediment diagenesis.

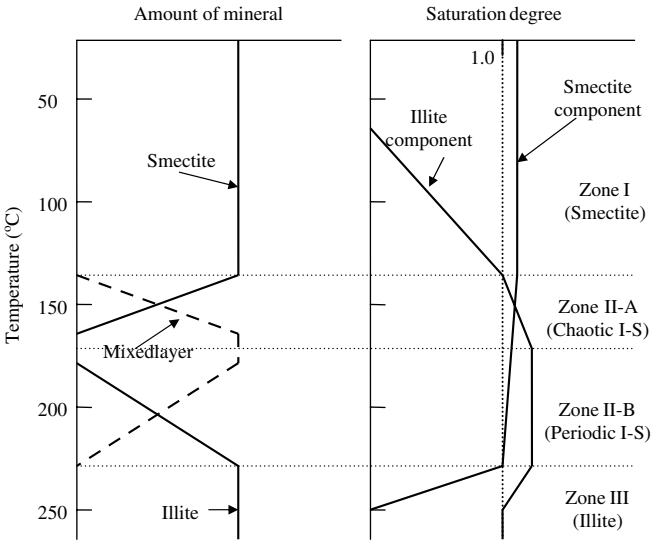

Fig. 8. Schematic representation of smectite (S)–illite (I) transition postulated from field observations and our modeling results. This transition is caused by relative changes in the saturation degree of pore water with respect to smectite and illite (Fig. 4C). The temperature interval for each mineral is based on the field observations by Inoue et al. (2004, Fig. 12).

4.5. Compositional gap and variable layer composition

In the foregoing discussions, we refer structural components as having two sets of (Si, Al)–O pseudo-hexagonal rings in the base T-sheet with distinct geometric distortions corresponding to end-member mineral phases. We assume that the relative proportion of each structural component can vary continuously over $[0, 1]$ from layer to layer. We want to point out that the chemical composition of the base T-sheet may also vary continuously from layer to layer and thus the structural components defined above may represent actual chemical species in the base T-sheet. Such an extension is necessary given the fact that a structural variation in the base T-sheet is, in many cases, associated with a change in chemical composition (e.g., various degrees of Al substitution for Si at tetrahedral sites). The concept of a continuous variation in chemical composition among silicate layers may first appear counter-intuitive, because of the existence of a large compositional gap between two uninterstratified phyllosilicate minerals, which has led us to infer that silicate layers in these mineral have fixed chemical compositions. The following model analysis, however, suggests that this may not be the case for interstratified minerals. Interestingly, our model can actually predict the observed compositional gap based on the assumption of a continuous compositional variation in the base T-sheet among the layers.

Let's assume that the structural configuration of the base T-sheet is now represented by the relative proportions of (Si, Al)–O tetrahedral units. The compositional changes in the base T-sheet from layer to layer can be modeled with the same set of Eqs. (1A), (1B), (2), (3), (4), (5), (6), (7), (8), (9). For simplicity, let's examine the cases where $\beta = 1$ and $\gamma = 1$. In order for Eq. (4) to have a stable steady state, it is required from Eqs. (7) and (8) that:

$$\alpha\overline{X} = (\alpha - 2)\Omega_A + 1, \tag{10}$$

$$\alpha < 6 - \frac{3}{\Omega_A}. \tag{11}$$

By eliminating Ω_A in the above equations, and also considering that the above equations should apply symmetrically to both structural components, we obtain

$$\overline{X} > \frac{2}{6-\alpha} \text{ or } \overline{X} < 1 - \frac{2}{6-\alpha} \tag{12}$$

Note that the composition of an uninterstratified mineral corresponds to a stable steady-state solution to Eq. (4). With a minimum value of α (=3.0) obtained from Fig. 4A, it is calculated from Eq. (12) that $\overline{X} > 67\%$ or $\overline{X} < 33\%$. This implies that the composition of an uninterstratified mineral must be close to that of the end-member phase and any intermediate bulk composition would inevitably lead to the formation of interstratified mineral phases. Thus, the compositional gap between two uninterstratified mineral phases is a natural outcome of nonlinear mineral growth kinetics. This prediction is consistent with field observations. For example, clay minerals intermediate in bulk composition between vermiculite and micas do not form layers of a single type but form mixed-layer structures with some low-charged layers interspersed among high-charged layers (Drever, 1982, p. 74). Similarly, as shown in Fig. 3, the molar fraction of pyrophyllite in the interstratified chlorite–pyrophyllite crystals ranges from 0.23 to 0.46, roughly falling in the predicted compositional gap. Traditionally, the observed compositional gap has been attributed to the limited solubility of solid solution between the end-member phases (e.g., Xu et al., 1996). Our model analysis, however, shows that the gap may not be a true thermodynamic immiscibility gap and instead it is a manifestation of coupled kinetic processes. To test this concept will require compositional measurements in individual phyllosilicate layers, which are probably difficult to obtain with existing microanalysis techniques.

The charges created by substitution of Al for Si in the base T-sheet in interstratified minerals are balanced by cations at both octahedral and interlayer sites as in normal clay minerals. Some unique characteristics can be expected for interstratified phyllosilicates, if the chemical composition in the base T-sheet varies continuously from layer to layer. Let's look at an extreme case—the chlorite–pyrophyllite system, in which macroscopic charge neutrality is maintained by stacking a certain number of $Al_{2.33}(OH)_6^+$ sheets onto appropriate 2:1 silicate layers during mineral precipitation. Since $Al_{2.33}(OH)_6^+$ sheets have a fixed charge density, the charge in each layer may not be exactly balanced for a variable base T-sheet composition, and thus a small local charge fluctuation may result. $Al_{2.33}(OH)_6^+$ sheets precipitate in such a way that the resulting local charge fluctuation is minimized, within ± 0.5 per $O_{10}(OH)_8$, and canceled out over a scale of a few layers, so that the macroscopic charge neutrality is maintained. This local charge fluctuation may be another factor, in addition to the structural strain energy, driving the system toward the precipitation of the like structural component as implied in Eq. (3). Regardless of the detail charge balance mechanisms, we expect that a periodic compositional variation in the base T-sheet requires periodic precipitation of $[Al_{2.33}(OH)_6]^+$ sheets (e.g., every two or three layers) in order to maintain macroscopic charge neutrality. Similarly, a chaotic compositional change requires aperiodic precipitation of $[Al_{2.33}(OH)_6]^+$ sheets. A silicate layer with a $[Al_{2.33}(OH)_6]^+$ sheet associated would exhibit typical characteristics of chlorite layer with a *d*-spacing of 14.2 Å.

5. Conclusions

We have demonstrated that interstratification in phyllosilicates can autonomously emerge from simple kinetics of mineral growth from an aqueous solution. The precipitation of individual silicate layers can be described by a one-dimensional map accounting for two competing factors: (1) the affinity for the attachment of each structural component onto a preceding silicate layer and (2) the strain energy created by stacking next to each other the two silicate layers with different structural configurations in *a*–*b* dimensions. Chaotic interstratification occurs when the contacting solution becomes slightly supersaturated with both structural components. The transition from one interstratification pattern to another reflects a change in chemical environment during mineral crystallization. Our model has successfully predicted the observed associations of mixed-layer mineral phases and layer stacking sequences in both hydrothermal alteration and sediment diagenesis. The structural transition of smectite to illite in sediment diagenesis reflects relative changes in the saturation degree of pore water with respect to two structural components as a result of temperature increases. Our model has also predicted the observed compositional gap between two uninterstratified mineral phases.

Acknowledgments

Sandia is a multi-program laboratory operated by Sandia Corporation, a Lockheed Martin Co., for the United States Department of Energy's (DOE) National Nuclear Security Administration under Contract DE-AC04-94AL85000. Authors thank Drs. Kathryn L. Nagy (Associate editor), D.D. Eberl, B. Sivakumar, H. Dong, and three anonymous reviewers for their constructive suggestions. Xu also thanks the WARF Foundation of University of Wisconsin-Madison for supporting this research.

Associate editor: Kathryn L. Nagy

References

Ahn, J.H., Peacor, D.R., 1986. Transmission and analytical electron microscopy of the smectite-to-illite transition. *Clays Clay Miner.* **34**, 165–179.

Alt, J.C., Jiang, W.-T., 1991. Hydrothermally precipitated mixed-layer illite-smectitie in recent massive sulfide deposits from the sea floor. *Geology* **19**, 570–573.

Altaner, S.P., Ylagan, R.F., 1997. Comparison of structural models of mixed-layer illite/smectite and reaction mechanisms of smectite illitization. *Clays Clay Miner.* **45**, 517–533.

Bailey, S.W., 1988. Chlorites: structures and crystal chemistry. In: *Hydrous Phyllosilicates (exclusive of micas)*. In: Bailey, S.W. (Ed.), *Reviews in Mineralogy*, vol. 19, pp. 347–403.

Bailey, S.W., Banfield, J.F., Barker, W.W., Katchan, G., 1995. Dozyite, a 1:1 regular interstratification of serpentine and chlorite. *Am. Mineral.* **80**, 65–77.

Baker, G.L., Gollub, J.P., 1990. *Chaotic Dynamics*. Cambridge University Press, New York, 182p.

Bautier, M.D., Fruhgreen, G.L., Karpoff, A.M., 1995. Mechanisms of Mg-phyllosilicate formation in a hydrothermal system at a sedimented ridge (Middle-Valley, Juan-De-Fuca). *Contrib. Mineral. Petrol.* **122**, 134–151.

Blanc, P., Bieber, A., Fritz, B., Duplay, J., 1997. A short range interaction model applied to illite/smectite mixed layer minerals. *Phys. Chem. Miner.* **24**, 574–581.

Berman, R.G., 1988. Internally-consistent thermodynamic data for minerals in the system Na_2O–K_2O–CaO–MgO–FeO–Fe_2O_3–Al_2O_3–SiO_2–TiO_2–H_2O–CO_2. *J. Petrol.* **29**, 445–522.

Burst, J.F., 1959. Post-diagenetic clay mineral environmental relationships in the Gulf Coast Eocene. *Clays Clay Miner.* **6**, 327–341.

Dekov, V.M., Scholten, J., Botz, R., Garbe-Schonberg, C.D., Thiry, M., Stoffers, P., Schmidt, M., 2005. Occurrence of kaolinite and mixed-layer kaolinite/smectite in hydrothermal sediments of Grimsey Graben, Tjornes Fracture Zone (north of Iceland). *Mar. Geol.* **215**, 159–170.

Dong, H., 2005. Interstratified illite–smectite: A review of contributions of TEM data to crystal chemical relations and reaction mechanisms. *Clay Sci.* **12** (Suppl. 1), 6–12.

Dong, H., Peacor, D.R., Merriman, R.J., Kemp, S.J., 2002. Brinrobertsite: A new RI interstratified pyrophyllite/smectite-like clay mineral: characterization and geological origin. *Mineral. Mag.* **66**, 605–617.

Drever, J.I., 1982. *The Geochemistry of Natural Waters*. Prentice-Hall, NJ, 388p.

Eberl, D.D., Środoń, J., Krailik, M., Taylor, B., Peterman, Z.E., 1990. Ostwald ripening of clays and metamorphic minerals. *Science* **248**, 474–477.

Eggleton, R.A., Banfield, J.F., 1985. The alteration of granitic biotite to chlorite. *Am. Mineral.* **70**, 902–910.

Eroshchev-Shak, V.A., 1970. Mixed-layer biotite–chlorite formed in course of local epigenesis in the weathering crust of biotite genesis. *Sedimentology* **15**, 115–121.

Evans, B.W., Guggenheim, S., 1988. Talc, pyrophyllite, and related minerals. In: *Hydrous Phyllosilicates (exclusive of micas)*. In: Bailey, S.W. (Ed.), *Reviews in Mineralogy*, vol. 19, pp. 225–294.

Hasse, C.S., Chadam, J., Feinn, D., 1980. Oscillatory zoning in plagioclase feldspar. *Science* **209**, 272–274.

Hiller, S., 1993. Origin, diagenesis, and mineralogy of chlorite minerals in Devonian Lacustrine mudrocks, Orcadian basin, Scotland. *Clays Clay Miner.* **41**, 240–259.

Hower, J., Eslinger, E.V., Hower, M.E., Perry, E.A., 1976. Mechanism of burial metamorphism of argillaceous sediments: 1. Mineralogical and chemical evidence. *Geol. Soc. Am. Bull.* **87**, 725–737.

Huang, J., Turcotte, D.L., 1990. Are earthquakes an example of deterministic chaos? *Geophys. Res. Lett.* **17**, 223–226.

Huang, J., Turcotte, D.L., 1992. Chaotic seismic faulting with a mass-spring model and velocity-weakening friction. *Pure Appl. Geophys.* **138**, 569–589.

Inoue, A., Meuiner, A., Beaufort, D., 2004. Illite-smectite mixed-layer minerals in felsic volcaniclastic rocks from drill cores, Kakkonda, Japan. *Clays Clay Miner.* **52**, 66–84.

Kong, Y., Peng, X., Tian, D., 1990. Lunijianlaite: A new regular interstratified mineral. *Acta Mineral. Sin.* **10**, 289–298.

Lasaga, A.C., 1981. Transition state theory Kinetics of Geochemical Processes. In: Lasaga, A.C., Kirkpatrick, R.J. (Eds.), *Reviews in Mineralogy*, vol. 8, pp. 69–110.

Lynch, F.L., Mack, L.E., Land, L.S., 1997. Burial diagenesis of illite/smectite in shales and the origins of authigenic quartz and secondary porosity in sandstones. *Geochim. Cosmochim. Acta* **61**, 1995–2006.

Maresch, W.V., Massonne, H.-J., Czank, M., 1985. Ordered and disordered chlorite/biotite interstratifications as alteration products of chlorite. *Neues Jahrb. Miner. Abh.* **152**, 79–100.

May, R., 1976. Simple mathematical model with very complicated dynamics. *Nature* **261**, 45–67.

Merino, E., Wang, Y., 2000. Geochemical self-organization in rocks: Occurrences, observations, modeling, testing—with emphasis on agate genesis. In: Krug, H.-J., Kruhl, J.H. (Eds.), *Non-Equilibrium Processes and Dissipative Structures in Geoscience*. Duncker & Humblot, Berlin, pp. 13–45.

Nadeau, P.H., Wilson, M.J., McHardy, W.J., Tait, J.M., 1984. Interstratified clays as fundamental particles. *Science* **225**, 923–935.

Niu, B., Yoshimura, T., Hira, A., 2000. Smectite diagenesis in Neogene marine sandston and mudstone of the Niigata Basin, Japan. *Clays Clay Miner.* **48**, 26–42.

Olives, J., Amouric, M., Perbost, R., 2000. Mixed layering of illite–smectite: Results from high-resolution transmission electron microscopy and lattice-energy calculations. *Clays Clay Miner.* **48**, 282–289.

Schreyer, W., Medenbach, O., Abraham, K., Gebert, W., Müller, W.F., 1982. Kulkeite, a new metamorphic phyllosilicate mineral: Order 1:1 chlorite/talc mixed-layer. *Contrib. Mineral. Petrol.* **80**, 103–109.

Sivakumar, B., 2004. Chaos theory in geophysics: past, present, and future. *Chaos Solitions Fractals* **19**, 441–462.

Sprott, J.C., 2003. *Chaos and Time-Series Analysis*. Oxford University Press, New York, 507p.

Środoń, J., 1999. Nature of mixed-layer clays and mechanisms of their formation and alteration. *Annu. Rev. Earth Planet. Sci.* **27**, 19–53.

Środoń, J., Eberl, D.D., 1984. Illite. In Micas (ed. S.W. Bailey), *Reviews of Mineralogy*, vol. 13, 495–544.

Środoń, J., Eberl, D.D., Drits, V.A., 2000. Evolution of fundamental-particle size during illitization of smectite and implications for reaction mechanism. *Clays Clay Miner.* **48**, 446–458.

Strogatz, W.H., 1994. *Nonlinear Dynamics and Chaos: With Applications to Physics, Biology, Chemistry, and Engineering*. Westview, Maryland, 498p.

Veblen, D.R., 1983. Microstructures and mixed layering in intergrown wonesite, chlorite, talc, biotite, and kaolinite. *Am. Mineral.* **65**, 566–580.

Veblen, D.R., Ferry, J.M., 1983. A TEM study of the biotite–chlorite reaction and comparison with petrologic observations. *Am. Mineral.* **68**, 1160–1168.

Veblen, D.R., Guthrie Jr., G.D., Livi, K.J.T., Reynolds Jr., R.C., 1990. High resolution transmission electron microscopy and electron diffraction of mixed-layer illite/smectite: Experimental results. *Clays Clay Miner.* **38**, 1–13.

Wang, Y., Merino, E., 1992. Dynamic model of oscillatory trace metal zoning in calcite: inhibition, double layer, and self-organization. *Geochim. Cosmochim. Acta* **56**, 587–596.

Wang, Y., Merino, E., 1993. Oscillatory magma crystallization by feedback between the concentrations of reactants and mineral growth. *J. Petrol.* **34**, 369–382.

Wang, Y., Merino, E., 1995. Origin of fibrosity and banding in agates from flood basalts. *Am. J. Sci.* **295**, 49–77.

Xu, H., Veblen, D.R., 1996. Interstratification and other reaction microstructures in the chlorite–berthierine series. *Contrib. Mineral. Petrol.* **124**, 291–301.

Xu, H., Zhang, Y., Veblen, D.R., 1996. Periodic and nonperiodic interstratification in the chlorite–biotite series. *Am. Mineral.* **81**, 1396–1404.

Zen, E., 1967. Mixed-layer minerals as one-dimensional crystals. *Am. Mineral.* **52**, 635–660.